Appl. Phys. B 47, 71–81 (1988)

Applied Physics B Photophysics and Laser Chemistry

Picosecond Third-Harmonic Light Generation in Calcite

A. Penzkofer, F. Ossig, and P. Qiu*

Naturwissenschaftliche Fakultät II – Physik, Universität, D-8400 Regensburg, Fed. Rep. Germany

Received 14 September 1987/Accepted 2 December 1987

Abstract. The third-harmonic generation of picosecond light pulses in a calcite crystal is studied experimentally and theoretically. A passively mode-locked Nd:phosphate glass laser is used in the experiments. The third-order nonlinear susceptibility components and the effective third-order nonlinear susceptibility of type II phase-matched (ooe→e) third-harmonic generation are determined.

PACS: 42.65C

Conversion of laser light to the third-harmonic frequency may be achieved by cascading second-order nonlinear optical processes or by direct application of a third-order nonlinear optical process. The cascading of phase-matched second-harmonic generation, $\omega_1+\omega_1\rightarrow\omega_2$, and phase-matched frequency mixing, $\omega_2+\omega_1\rightarrow\omega_3$, in two separate crystals without inversion symmetry is an efficient technique of light generation at the third-harmonic frequency $\omega_3=3\omega_1$ [1–3]. Direct phase-matched third-harmonic generation in gases (rare gases, metal vapors) is applied to generate vacuum ultraviolet coherent radiation [4–6]. The efficient third-harmonic generation in some phase-matched organic dye solutions was analysed recently [7–10]. The phase-matched third-harmonic generation in a single crystal without inversion center is possible by cascading second-order effects and by combining second-order effects and direct third-harmonic generation [11–13]. In birefringent crystals with inversion symmetry second-order processes are parity forbidden but direct third-harmonic generation is allowed and angular phase-matching is possible [11, 13–16].

In this paper the phase-matched direct third-harmonic generation in calcite is studied [11, 13–16]. Calcite is an uniaxial crystal of trigonal crystal symmetry (space group $R\bar{3}c$, point group $\bar{3}m$). It has an inversion center. Picosecond pump pulses of a passively mode-locked Nd-phosphate glass laser are applied. Type-II phase-matching is applied (ooe→e interaction with phase-matching angle $\Theta=36°$, o: ordinary ray; e: extraordinary ray). The energy conversion versus pump pulse peak intensity is measured. The relevant third-order nonlinear susceptibility components and the effective nonlinear third-order nonlinear susceptibility $\chi^{(3)}_{\text{eff},II}$ are determined. The influences of spectral width, beam divergence, and beam diameter on the third-harmonic conversion efficiency are analysed.

1. Theory

The third-harmonic generation is described by the nonlinear wave equation [17–19]

$$\nabla\times\nabla\times\mathbf{E}+\frac{\overleftrightarrow{\varepsilon}}{c_0^2}\frac{\partial^2}{\partial t^2}\mathbf{E}=-\mu_0\frac{\partial^2}{\partial t^2}\mathbf{P}_{\text{NL}} \tag{1}$$

with

$$\mathbf{E}=\tfrac{1}{2}\{E_1\exp[\mathrm{i}(\omega_1 t-\mathbf{k}_1\mathbf{r})]\mathbf{e}_1 + E_3\exp[\mathrm{i}(\omega_3 t-\mathbf{k}_3\mathbf{r})]\mathbf{e}_3+\text{c.c.}\} \tag{2}$$

and

$$\mathbf{P}_{\text{NL}}=\tfrac{1}{2}\{\mathbf{P}_{\text{NL},1}\exp[\mathrm{i}(\omega_1 t-\mathbf{k}_1^p\mathbf{r})] + \mathbf{P}_{\text{NL},3}\exp[\mathrm{i}(\omega_3 t-\mathbf{k}_3^p\mathbf{r})]+\text{c.c.}\}. \tag{3}$$

* On leave from Shanghai Institute of Optics and Fine Mechanics, Academia Sinica, Shanghai, P.R. China

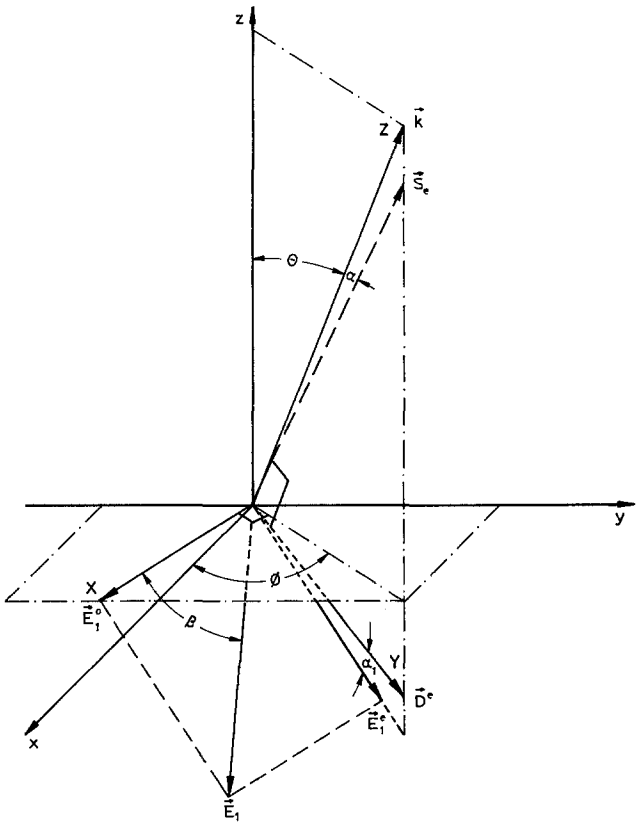

Fig. 1. Light propagation in crystal-fixed (xyz)-frame and in laboratory (XYZ)-frame. z is parallel to optical axis of calcite

$\overleftrightarrow{\varepsilon}$ is the relative permittivity tensor. μ_0 is the vacuum permeability. c_0 is the vacuum light velocity. E_1 and E_3 are the electrical field strengths of the pump laser (circular frequency ω_1) and of the third harmonic light ($\omega_3=3\omega_1$), respectively. $\mathbf{k}_1$ and $\mathbf{k}_3$ are the corresponding wavevectors. $\mathbf{e}_1$ and $\mathbf{e}_3$ are unit vectors. $\mathbf{P}_{\mathrm{NL},1}$ and $\mathbf{P}_{\mathrm{NL},3}$ are the third-order nonlinear polarizations at the circular frequencies ω_1 and ω_3, respectively.

Neglecting pump pulse depletion ($E_1=\text{const}$), selecting pump pulse propagation in Z direction, and using the slowly varying amplitude approximation (1) reduces to [20–22]

$$k_3\cos^2\alpha_3\frac{\partial E_3}{\partial Z}+\frac{\omega_3}{c_0^2}\mathbf{e}_3\overleftrightarrow{\varepsilon}_3\mathbf{e}_3\frac{\partial E_3}{\partial t}$$
$$=-\mathrm{i}\frac{\mu_0\omega_3^2}{2}\mathbf{e}_3\mathbf{P}_{\mathrm{NL},3}\exp(\mathrm{i}\Delta kZ); \tag{4}$$

α_3 is the walk-off angle between wave-vector direction $\mathbf{k}_3$ and ray direction $\mathbf{s}_{e3}$ of the third-harmonic light (Fig. 1). $\Delta k=k_3-k_3^p$ is the magnitude of the wave-vector mismatch. The transformations

$$t'=t-[\omega_3\mathbf{e}_3\overleftrightarrow{\varepsilon}_3\mathbf{e}_3/(c_0^2k_3\cos^2\alpha_3)]Z$$

and $Z'=Z$ reduce (4) to

$$\frac{\partial E_3}{\partial Z'}=-\mathrm{i}\frac{\mu_0\omega_3^2}{2k_3\cos^2\alpha_3}\mathbf{e}_3\mathbf{P}_{\mathrm{NL},3}\exp(\mathrm{i}\Delta kZ')$$
$$=-\mathrm{i}\frac{\mu_0\omega_3 c_0}{2n_3\cos^2\alpha_3}\mathbf{e}_3\mathbf{P}_{\mathrm{NL},3}\exp(\mathrm{i}\Delta kZ'). \tag{5}$$

For the last equality the relation $k_3=n_3\omega_3/c_0$ has been used. n_3 is the refractive index at the circular frequency ω_3.

The dispersion of the refractive index causes phase-mismatching. In the uniaxial crystal calcite collinear phase matching, $\Delta k=0$, is possible by angle tuning. Figure 1 depicts the light-propagation scheme in calcite. (x, y, z) represents the rectangular crystal-fixed coorindate system. The z-axis is parallel to the optical axis (c-axis). The wavefront propagation is parallel to $\mathbf{k}$ ($\mathbf{k}\perp\mathbf{D}$, $\mathbf{D}$ is dielectric displacement, Z-axis). The ray propagation (energy flow direction) is parallel to $\mathbf{s}$ ($\mathbf{s}\perp\mathbf{E}$). The electrical field strength of the ordinary ray, $\mathbf{E}^o$, is oriented perpendicular to the $(z, \mathbf{k})$-plane ($\mathbf{D}^o\parallel\mathbf{E}^o$, $\mathbf{k}_o\parallel\mathbf{s}_o$). The electrical field strength of the extraordinary ray, $\mathbf{E}^e$, is located in the $(z, \mathbf{k})$-plane ($\mathbf{D}^e\perp\mathbf{k}_e$, $\mathbf{k}_e\parallel\mathbf{k}_o\parallel\mathbf{k}$, $\mathbf{E}^e\perp\mathbf{s}$, $\angle(\mathbf{k},\mathbf{s}_e)=\angle(\mathbf{D}^e,\mathbf{E}^e)=\alpha$). The vectors $\mathbf{E}^o$, $\mathbf{D}^e$, and $\mathbf{k}$ span the rectangular (X, Y, Z) laboratory coordinate system.

The dispersion of the principle refractive indices, n_o and n_e, of calcite is depicted in Fig. 2 [23] (negative uniaxial crystal). Phase-matching is achieved by adjusting the angle θ between optical axis z and wave-vector $\mathbf{k}$. Three different phase-matching configurations are possible by applying different combinations of ordinary and extraordinary rays: Type-I phase-matching applies ooo→e interaction, type-II phase-matching uses ooe→e interaction, and type-III phase-matching is achieved by oee→e interaction [24]. The azimuthal angle ϕ does not influence the phase-matching, but it influences the effective nonlinear susceptibility (see below).

The phase-matching angle θ for collinear ooo→e interaction (type I) is found by the relation

$$\Delta k=k_{e3}-3k_{o1}=6\pi\tilde{\nu}_1[n_{e3}(\theta_I)-n_{o1}]=0 \tag{6}$$

($k_3^p=3k_{o1}$). The extraordinary refractive index at angle θ is given by

$$n_e(\theta)=\frac{n_o n_e}{(n_e^2\cos^2\theta+n_o^2\sin^2\theta)^{1/2}}. \tag{7}$$

Insertion of (7) into (6) gives

$$\theta_I=\arccos\left[\frac{n_{o3}}{n_{o1}}\left(\frac{n_{e3}^2-n_{o1}^2}{n_{e3}^2-n_{o3}^2}\right)^{1/2}\right]. \tag{8}$$

The refractive index data of calcite give a phase-matching angle of $\theta_I=29.64°$ for a pump laser wavelength of $\lambda_1=1.054\,\mu\mathrm{m}$.

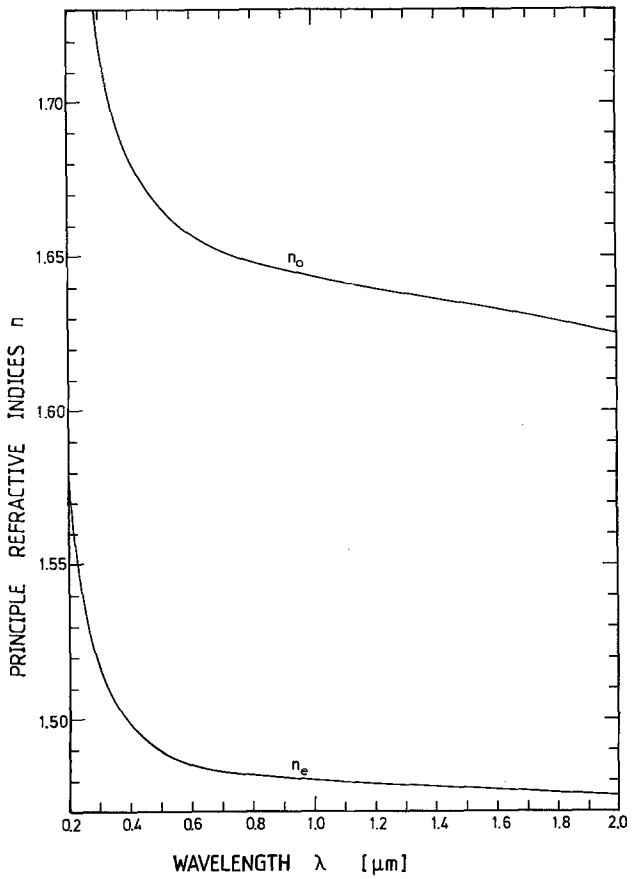

Fig. 2. Dispersion of principle refractive indices of calcite (from [23])

The phase-matching angle for the collinear ooe→e interaction (type II) is obtained from the relation

$$\Delta k = k_{e3} - 2k_{o1} - k_{e1} = 2\pi\tilde{\nu}_1[3n_{e3}(\theta_{II}) - 2n_{o1} - n_{e1}(\theta_{II})] = 0 \quad (9)$$

($k_3^p = 2k_{o1} + k_{e1}$). Equation (9) is solved numerically. A phase-matching angle of $\theta_{II} = 35.96°$ is obtained for $\lambda_1 = 1.054\,\mu m$.

The phase-matching angle for the collinear oee→e interaction (type III) is determined by the relation

$$\Delta k = k_{e3} - k_{o1} - 2k_{e1} = 2\pi\tilde{\nu}_1[3n_{e3}(\theta_{III}) - n_{o1} - 2n_{e1}(\theta_{III})] = 0 \quad (10)$$

($k_3^p = k_{o1} + 2k_{e1}$). The phase-matching angle is $\theta_{III} = 50.16°$ for $\lambda_1 = 1.054\,\mu m$.

The phase-matching angles θ_I, θ_{II}, and θ_{III} versus wavelengths λ_1 and λ_3 are depicted in Fig. 3a. The crystal is transparent between 200 nm and 2.2 μm [25]. Within this wavelength region type I and type II phase-matching are possible ($0.6\,\mu m \leqq \lambda_1 \leqq 2.2\,\mu m$; $200\,nm \leqq \lambda_3 \leqq 730\,nm$). The type III phase-matching is limited to $\lambda_1 \geqq 720\,nm$ ($\lambda_3 \geqq 240\,nm$).

The walk-off angle α between ray direction **s** and wavevector direction **k** (Fig. 1) of extraordinary polarized light is given by [22]

$$\tan\alpha = \tfrac{1}{2}\sin(2\theta)n_e^2(\theta)\left(\frac{1}{n_e^2} - \frac{1}{n_o^2}\right). \quad (11)$$

The walk-off angles α_1 and α_3 versus wavelength are depicted in Fig. 3b for type-II phase-matching.

The third-order nonlinear polarization, $\mathbf{P}_{NL}$, of (1) is given by [26]

$$\mathbf{P}_{NL} = 4\varepsilon_0 \vec{\vec{\chi}}^{(3)} : \mathbf{EEE}. \quad (12)$$

The third-order nonlinear polarization, $\mathbf{P}_{NL,3}$, of (3) reads

$$\mathbf{P}_{NL,3} = \varepsilon_0 E_{1a} E_{1b} E_{1c} \vec{\vec{\chi}}^{(3)} (-\omega_3; \omega_1, \omega_1, \omega_1) : \mathbf{e}_{1a}\mathbf{e}_{1b}\mathbf{e}_{1c} \quad (13a)$$

or

$$\mathbf{P}_{NL,e,i} = \varepsilon_0 E_{1a} E_{1b} E_{1c} \sum_{j,k,l=x,y,z} \chi_{ijkl}^{(3)} (-\omega_3; \omega_1, \omega_1, \omega_1) e_{1a,j} e_{1b,k} e_{1c,l}. \quad (13b)$$

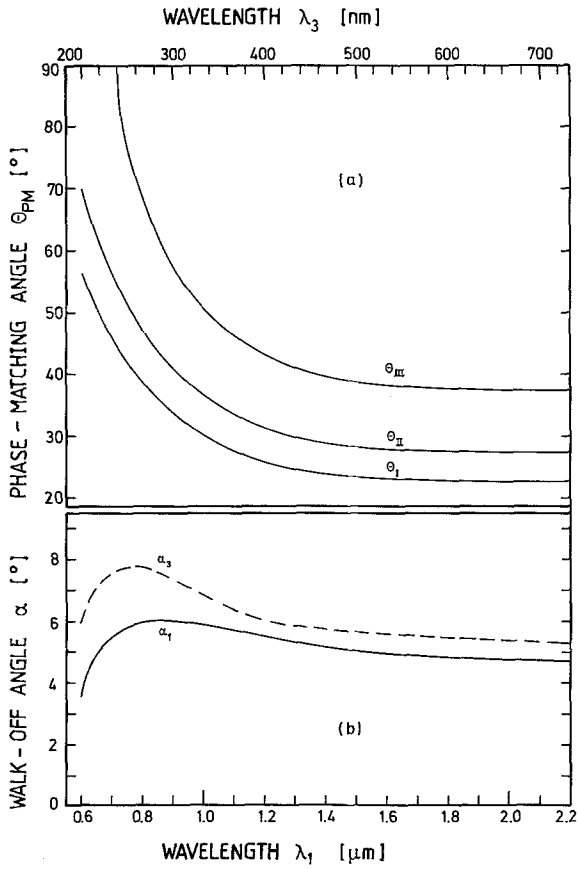

Fig. 3. (a) Phase-matching angle versus wavelength for type-I (θ_I, ooo→e), type-II (θ_{II}, ooe→e), and type-III phase-matching (θ_{III}, oee→e). (b) Walk-off angles α_1 (wavelength λ_1) and α_3 (wavelength λ_3) for type-II phase-matching

$\mathbf{E}_{1a}=E_{1a}\mathbf{e}_{1a}$, $\mathbf{E}_{1b}=E_{1b}\mathbf{e}_{1b}$, and $\mathbf{E}_{1c}=E_{1c}\mathbf{e}_{1c}$ are the electrical field strengths of the pump light at frequency ω_1. $\mathbf{e}_{1a}$, $\mathbf{e}_{1b}$, and $\mathbf{e}_{1c}$ represent unit vectors.

In case of ooo→e phase-matched third-harmonic generation (type I) it is $\mathbf{E}_{1a}=\mathbf{E}_{1b}=\mathbf{E}_{1c}=E_1^o\mathbf{e}_{o1}$ with

$$E_1^o(X,Y,t')=E_{10}\exp\left(-\frac{X^2+Y^2}{2r_0^2}\right)\exp\left(-\frac{t'^2}{2t_0^2}\right). \quad (14)$$

In case of ooe→e phase-matched third-harmonic generation (type II) it is $\mathbf{E}_{1a}=\mathbf{E}_{1b}=E_1^o\mathbf{e}_{o1}$ and $\mathbf{E}_{1c}=E_1^e\mathbf{e}_{e1}$. $\mathbf{P}_{NL,3}$ becomes maximal for $E_1^o=2E_1^e$ ($\beta_{II}=$arccotan(2)$=26.57°$, see Fig. 1). E_1^o and E_1^e are given by

$$E_1^o(X,Y,t')=E_{10}\cos(\beta_{II})\exp\left(-\frac{X^2+Y^2}{2r_0^2}\right)\times\exp\left(-\frac{t'^2}{2t_0^2}\right), \quad (15a)$$

$$E_1^e(X,Y,Z,t')=E_{10}\sin(\beta_{II})\times\exp\left[-\frac{X^2+(Y+\alpha_1 Z)^2}{2r_0^2}\right]\times\exp\left(-\frac{t'^2}{2t_0^2}\right). \quad (15b)$$

For oee→e phase-matched interaction it is $\mathbf{E}_{1a}=E_1^o\mathbf{e}_{o1}$ and $\mathbf{E}_{1b}=\mathbf{E}_{1c}=E_1^e\mathbf{e}_{e1}$. $\mathbf{P}_{NL,3}$ becomes maximal for $E_1^o=E_1^e/2$ ($\beta_{III}=$arctan(2)$=63.43°=90°-\beta_{II}$, see Fig. 1). E_1^o and E_1^e are given by

$$E_1^o(X,Y,t')=E_{10}\cos(\beta_{III})\exp\left(-\frac{X^2+Y^2}{2r_0^2}\right)\times\exp\left(-\frac{t'^2}{2t_0^2}\right) \quad (16a)$$

$$E_1^e(X,Y,Z,t')=E_{10}\sin(\beta_{III})\times\exp\left[-\frac{X^2+(Y+\alpha_1 Z)^2}{2r_0^2}\right]\times\exp\left(-\frac{t'^2}{2t_0^2}\right). \quad (16b)$$

Gaussian pulse shapes are assumed.

Insertion of (13a) into (5) gives

$$\frac{\partial E_3}{\partial Z'}=-\mathrm{i}\frac{\omega_3}{2n_3c_0\cos^2\alpha_3}E_{1a}E_{1b}E_{1c}\chi_{\mathrm{eff}}^{(3)}\times\exp(\mathrm{i}\Delta kZ') \quad (17)$$

with

$$\chi_{\mathrm{eff}}^{(3)}=\mathbf{e}_3\chi^{(3)}(-\omega_3;\omega_1,\omega_1,\omega_1)\vdots\mathbf{e}_{1a}\mathbf{e}_{1b}\mathbf{e}_{1c} \quad (18)$$

$c_0^2=(\mu_0\varepsilon_0)^{-1}$ is used. Neglecting the effect of the walk-off angle α_1 (15b and 16b) the integration of (17) gives for $E_3(0)=0$

$$E_3(l)=-\mathrm{i}\frac{\omega_3}{2n_3c_0\cos^2\alpha_3}E_{1a}E_{1b}E_{1c}\chi_{\mathrm{eff}}^{(3)}\times\frac{\exp(\mathrm{i}\Delta kl)-1}{\mathrm{i}\Delta k}=-\mathrm{i}\frac{\omega_3 l}{2n_3c_0\cos^2\alpha_3}E_{1a}E_{1b}E_{1c}\chi_{\mathrm{eff}}^{(3)}\times\exp\left(\frac{\mathrm{i}\Delta kl}{2}\right)\frac{\sin(\Delta kl/2)}{\Delta kl/2}. \quad (19)$$

The generated third-harmonic intensity is obtained by using the relation $I=(nc_0\varepsilon_0/2)\,|E|^2$:

$$I_3(l)=\frac{\omega_3^2 l^2}{n_3n_{1a}n_{1b}n_{1c}c_0^4\varepsilon_0^2\cos^4\alpha_3}I_{1a}I_{1b}I_{1c}|\chi_{\mathrm{eff}}^{(3)}|^2\times\frac{\sin^2(\Delta kl/2)}{(\Delta kl/2)^2}. \quad (20)$$

The energy conversion of third-harmonic light generation is given by

$$\eta=W_3(l)/W_1(0)=\left[\int_{-\infty}^{\infty}dX\int_{-\infty}^{\infty}dY\int_{-\infty}^{\infty}dt'I_3(l,X,Y,t')\right]\Big/\left[\int_{-\infty}^{\infty}dX\int_{-\infty}^{\infty}dY\int_{-\infty}^{\infty}dt'I_1(0,X,Y,t')\right].$$

For type-I interaction (ooo→e) (14) the energy conversion becomes [19]

$$\eta_I=\frac{1}{3^{3/2}}\frac{\omega_3^2l^2I_{10}^2|\chi_{\mathrm{eff},I}^{(3)}|^2}{n_{e3}(\theta_I)n_{o1}^3c_0^4\varepsilon_0^2\cos^4\alpha_3}\times\frac{\sin^2(\Delta kl/2)}{(\Delta kl/2)^2}, \quad (21a)$$

for type-II interaction (ooe→e) (15a and 15b)

$$\eta_{II}=\frac{1}{3^{3/2}}\cos^4(\beta_{II})\sin^2(\beta_{II})\times\frac{\omega_3^2l^2I_{10}^2|\chi_{\mathrm{eff},II}^{(3)}|^2}{n_{e3}(\theta_{II})n_{o1}^2n_{e1}(\theta_{II})c_0^4\varepsilon_0^2\cos^4\alpha_3}\times\frac{\sin^2(\Delta kl/2)}{(\Delta kl/2)^2}, \quad (21b)$$

and for type-III-Interaction (oee→e) (16a and 16b)

$$\eta_{III}=\frac{1}{3^{3/2}}\cos^2(\beta_{III})\sin^4(\beta_{III})\times\frac{\omega_3^2l^2I_{10}^2|\chi_{\mathrm{eff},III}^{(3)}|^2}{n_{e3}(\theta_{III})n_{o1}n_{e1}^2(\theta_{III})c_0^4\varepsilon_0^2\cos^4\alpha_3}\times\frac{\sin^2(\Delta kl/2)}{(\Delta kl/2)^2}. \quad (21c)$$

I_{10} is the input pulse intensity inside the crystal. In the experiments the reflection losses have to be separately

considered. In the case of phase-matching, $\Delta k=0$, one has $\sin^2(\Delta kl/2)/(\Delta kl/2)^2=1$.

The effective nonlinear susceptibilities $\chi^{(3)}_{\mathrm{eff},I}$, $\chi^{(3)}_{\mathrm{eff},II}$, used $\chi^{(3)}_{\mathrm{eff},III}$ are found by the following considerations. Setting $i=1,2,3$ for $i=x,y,z$ and using the contractions [24] $1=xxx$, $2=yyy$, $3=zzz$, $4=yzz$, $5=yyz$, $6=xzz$, $7=xxz$, $8=xyy$, $9=xxy$, $0=xyz$ for jkl [see (13b)], the effective third-order nonlinear susceptibility, $\chi^{(3)}_{\mathrm{eff}}$ (18), of calcite ($\bar{3}m$ point group) may be rewritten to

$$\chi^{(3)}_{\mathrm{eff}}=\mathbf{e}_3\overleftrightarrow{\chi}^{(3)}\mathbf{e}_{111} \tag{22}$$

with

$$\mathbf{e}_3=(e_{3x},e_{3y},e_{3z}) \tag{23}$$

$$\overleftrightarrow{\chi}^{(3)}=\begin{pmatrix} \chi_{11} & 0 & 0 & 0 & 0 & \chi_{16} & 0 & \frac{1}{3}\chi_{11} & 0 & \chi_{10} \\ 0 & \chi_{11} & 0 & \chi_{16} & -\chi_{10} & 0 & \chi_{10} & 0 & \frac{1}{3}\chi_{11} & 0 \\ 0 & -\chi_{39} & \chi_{33} & 0 & \chi_{35} & 0 & \chi_{35} & 0 & \chi_{39} & 0 \end{pmatrix} \tag{24}$$

and

$$\mathbf{e}_{111}=\begin{pmatrix} e_{1ax}e_{1bx}e_{1cx} \\ e_{1ay}e_{1by}e_{1cy} \\ e_{1az}e_{1bz}e_{1cz} \\ e_{1az}e_{1bz}e_{1cy}+e_{1az}e_{1by}e_{1cz}+e_{1ay}e_{1bz}e_{1cz} \\ e_{1ay}e_{1by}e_{1cz}+e_{1ay}e_{1bz}e_{1cy}+e_{1az}e_{1by}e_{1cy} \\ e_{1az}e_{1bz}e_{1cx}+e_{1az}e_{1bx}e_{1cz}+e_{1ax}e_{1bz}e_{1cz} \\ e_{1ax}e_{1bx}e_{1cz}+e_{1ax}e_{1bz}e_{1cx}+e_{1az}e_{1bx}e_{1cx} \\ e_{1ay}e_{1by}e_{1cx}+e_{1ay}e_{1bx}e_{1cy}+e_{1ax}e_{1by}e_{1cy} \\ e_{1ax}e_{1bx}e_{1cy}+e_{1ax}e_{1by}e_{1cx}+e_{1ay}e_{1bx}e_{1cx} \\ \sum\limits_{j\neq k\neq l=x,y,z} e_{1aj}e_{1bk}e_{1cl} \end{pmatrix}. \tag{25}$$

The unit vectors $\mathbf{e}_o$ and $\mathbf{e}_e$ of the ordinary and extraordinary field strenghts are given by

$$\mathbf{e}_o=\begin{pmatrix} \sin\phi \\ -\cos\phi \\ 0 \end{pmatrix} \tag{26}$$

and

$$\mathbf{e}_e=\begin{pmatrix} \cos(\theta+\alpha)\cos\phi \\ \cos(\theta+\alpha)\sin\phi \\ -\sin(\theta+\alpha) \end{pmatrix} \tag{27}$$

in the (x,y,z) crystal frame. The susceptibility tensor, $\overleftrightarrow{\chi}^{(3)}$, of calcite is taken from [22, 24, 28]. The Kleinman symmetry condition [27] simplifies the $\overleftrightarrow{\chi}^{(3)}$ tensor components to $\chi_{39}=\chi_{10}$ and $\chi_{35}=\chi_{16}$ [24].

For ooo→e interaction the application of (22–27) gives

$$\chi^{(3)}_{\mathrm{eff},I}=\chi_{39}\sin(\theta_I+\alpha_3)\cos(3\phi). \tag{28}$$

In case of ooe→e interaction, the effective nonlinear susceptibility is

$$\begin{aligned}\chi^{(3)}_{\mathrm{eff},II}=&[\tfrac{1}{3}\chi_{11}\cos(\theta_{II}+\alpha_1)+\chi_{10}\sin(\theta_{II}+\alpha_1)\\ &\times\sin(3\phi)]\cos(\theta_{II}+\alpha_3)+[\chi_{35}\sin(\theta_{II}+\alpha_1)\\ &+\chi_{39}\cos(\theta_{II}+\alpha_1)\sin(3\phi)]\sin(\theta_{II}+\alpha_3).\end{aligned} \tag{29}$$

The effective nonlinear susceptibility for oee→e interaction is

$$\begin{aligned}\chi^{(3)}_{\mathrm{eff},III}=&\{\chi_{10}\sin[2(\theta_{III}+\alpha_1)]\cos(\theta_{III}+\alpha_3)\\ &+\chi_{39}\cos^2(\theta_{III}+\alpha_1)\sin(\theta_{III}+\alpha_3)\}\cos(3\phi).\end{aligned} \tag{30}$$

Type-I third-harmonic generation is caused by the coupling constant

$$\chi_{10}=\chi^{(3)}_{xxyz}(-\omega_3;\omega_1,\omega_1,\omega_1).$$

$\chi^{(3)}_{\mathrm{eff},I}$ has a maximum for $\phi=0°$ and it is zero for $\phi=90°$ and 270°. Type-II third-harmonic generation has contributions from

$$\chi_{11}=\chi^{(3)}_{xxxx}(-\omega_3;\omega_1,\omega_1,\omega_1),$$
$$\chi_{10}=\chi^{(3)}_{xxyz}(-\omega_3;\omega_1,\omega_1,\omega_1),$$
$$\chi_{35}=\chi^{(3)}_{zyyz}(-\omega_3;\omega_1,\omega_1,\omega_1)$$

and

$$\chi_{39}=\chi^{(3)}_{zxxy}(-\omega_3;\omega_1,\omega_1,\omega_1)(\chi_{39}=\chi_{10}).$$

Type-III third-harmonic generation is caused by χ_{10} and χ_{39} (Kleinman symmetry: $\chi_{10}=\chi_{39}$). $\chi^{(3)}_{\mathrm{eff},III}$ has a maximum for $\phi=0°$ and it is zero for $\phi=90°$ and 270°.

The conversion efficiency of phase-matched third-harmonic generation is reduced by the beam divergence, the beam diameter, and the spectral bandwidth of the pump pulse.

The ratio of energy conversion, $\eta(\Delta\theta)/\eta(0)$, of a pump pulse of beam divergence angle $\Delta\theta$ (FWHM) and of a non-divergent pulse ($\Delta\theta=0$) is approximately given by

$$\frac{\eta(\Delta\theta)}{\eta(0)}=\frac{\int_0^\infty \exp[-(\theta'/\theta_0)^2]\dfrac{\sin^2\left(\dfrac{\partial\Delta k}{\partial\theta'}\theta' l/2\right)}{\left(\dfrac{\partial\Delta k}{\partial\theta'}\theta' l/2\right)^2}d\theta'}{\int_0^\infty \exp[-(\theta'/\theta_0)^2]d\theta'} \tag{31}$$

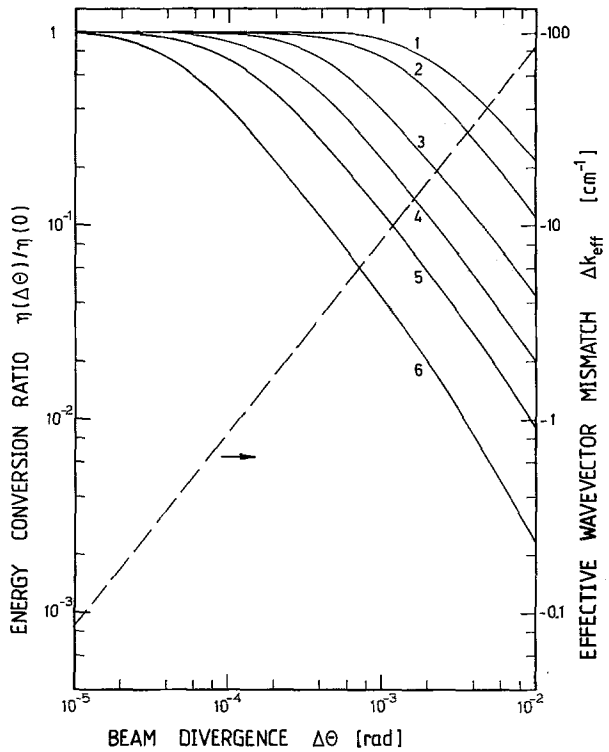

Fig. 4. Reduction of third-harmonic energy conversion efficiency by pump pulse divergence $\Delta\theta$ (FWHM, in crystal) for type-II phase-matching. Curves *1* $l=0.1$ cm; *2* $l=0.2$ cm; *3* $l=0.5$ cm; *4* $l=1$ cm; *5* $l=2$ cm; *6* $l=5$ cm. Effective wave-vector mismatch due to beam divergence is included (dashed curve). $\lambda_1=1.054\,\mu$m

with $\theta_0=\Delta\theta/\{2[\ln(2)]^{1/2}\}$. The value of the integral in the denominator is $(\pi^{1/2}/2)\theta_0$. The angular derivative of the wave-vector mismatch is

$$\partial\Delta k/\partial\theta' \simeq -2.5\times10^4\,\mathrm{cm}^{-1}\,\mathrm{rad}^{-1}$$

at the phase-matching angle $\theta_{II}=35.96°$. In Fig. 4 the reduction of energy conversion versus pump pulse divergence $\Delta\theta$ is plotted for various sample lengths (ooe→e interaction). For a crystal length of $l=2$ cm and a laser beam divergence of $\Delta\theta=5\times10^{-4}$ rad the reduction of the energy conversion is $\eta(\Delta\theta)/\eta(0)=0.22$. $\Delta\theta$ is the beam divergence (FWHM) inside the crystal. It is related to the beam divergence outside the crystal by $\Delta\theta_{\mathrm{out}}\simeq n_{o1}\Delta\theta$.

An effective wave-vector mismatch, Δk_{eff}, due to the laser pulse divergence may be determined by

$$\Delta k_{\mathrm{eff}}=\frac{\int_0^\infty \exp[-(\theta'/\theta_0)^2]\frac{\partial\Delta k}{\partial\theta'}\theta'd\theta'}{\int_0^\infty \exp[-(\theta'/\theta_0)^2]d\theta'}=\frac{1}{2[\pi\ln(2)]^{1/2}}\frac{\partial\Delta k}{\partial\theta}\Delta\theta. \tag{32}$$

$\Delta k_{\mathrm{eff}}(\Delta\theta)$ is included in Fig. 4 (dashed line). The pump laser may be focused to a line in the YZ plane in order to increase the pump pulse intensity without increasing the relevant beam divergence.

The reduction of energy conversion due to the spectral bandwidth $\Delta\tilde{\nu}$ (FWHM) of the pump pulse is approximately given by the ratio

$$\frac{\eta(\Delta\tilde{\nu})}{\eta(0)}=\frac{\int_0^\infty \exp[-(\tilde{\nu}'/\tilde{\nu}_0)^2]\frac{\sin^2\left(\frac{\partial\Delta k'}{\partial\tilde{\nu}'}\tilde{\nu}'l/2\right)}{\left(\frac{\partial\Delta k'}{\partial\tilde{\nu}'}\tilde{\nu}'l/2\right)^2}d\tilde{\nu}'}{\int_0^\infty \exp[-(\tilde{\nu}'/\tilde{\nu}_0)^2]d\tilde{\nu}'} \tag{33}$$

with $\tilde{\nu}_0=\Delta\tilde{\nu}/\{2[\ln(2)]^{1/2}\}$.

The value of the integral in the denominator is $(\pi^{1/2}/2)\tilde{\nu}_0$. The frequency derivative $\partial\Delta k/\partial\tilde{\nu}$ at the ooe→e phasematching angle is $\partial\Delta k/\partial\tilde{\nu}=1.38\,\mathrm{cm}^{-1}/\mathrm{cm}^{-1}$. Besides the third harmonic process $\omega_1+\omega_1+\omega_1\to\omega_3$, the frequency mixing $\omega_1+(\omega_1-\delta\omega)+(\omega_1+\delta\omega)\to\omega_3$ contributes to light generation at $\omega_3(\delta\omega\lesssim\Delta\omega=2\pi c_0\Delta\tilde{\nu})$. The frequency mixing reduces the wave-vector mismatch. For bandwidth limited pulses it is assumed that the spectral width of the third-harmonic light is about the same as the spectral width of the pump pulse and the frequency derivative of the wave-vector mismatch is approximated by $\partial\Delta k'/\partial\tilde{\nu}\simeq(1/3)\partial\Delta k/\partial\tilde{\nu}$. For chirped pulses (self-phase-modulated pulses) [29–32] the pulse spectrum changes with time and only third-harmonic generation is relevant ($\partial\Delta k'/\partial\tilde{\nu}\simeq\partial\Delta k/\partial\tilde{\nu}$).

The reduction of energy conversion $\eta(\Delta\tilde{\nu})/\eta(0)$ versus spectral width $\Delta\tilde{\nu}$ is plotted in Fig. 5 for some sample lengths. The lower abscissa belongs to the spectral width of chirped pulses ($\partial\Delta k'/\partial\tilde{\nu}=1.38$). The upper abscissa belongs to bandwidth-limited Gaussian pulses ($\partial\Delta k'/\partial\tilde{\nu}=0.46$). The pulse duration Δt of the pump pulse (FWHM) is indicated. It is related to the spectral bandwidth $\Delta\tilde{\nu}$ (FWHM) by $\Delta t=[2\ln(2)/\pi]/(\Delta\tilde{\nu}c_0)$ [34]. For a bandwidth-limited pulse of 5 ps duration the third-harmonic energy in a 2 cm long calcite crystal is reduced to $\eta(\Delta\tilde{\nu})/\eta(0)=0.9$. For a self-phase-modulated pulse of $\Delta\tilde{\nu}=20\,\mathrm{cm}^{-1}$ the energy conversion in a 2 cm long calcite crystal reduces to $\eta(\Delta\nu)/\eta(0)=0.1$.

An effective wave-vector mismatch due to the spectral width of the pump laser may be defined by

$$\Delta k_{\mathrm{eff}}=\frac{\int_0^\infty \exp[-(\tilde{\nu}'/\tilde{\nu}_0)^2]\frac{\partial\Delta k'}{\partial\tilde{\nu}'}\tilde{\nu}'d\tilde{\nu}}{\int_0^\infty \exp[-(\tilde{\nu}'/\tilde{\nu}_0)^2]d\tilde{\nu}'}=\frac{1}{2[\pi\ln(2)]^{1/2}}\frac{\partial\Delta k'}{\partial\tilde{\nu}}\Delta\tilde{\nu}. \tag{34}$$

The $\Delta k_{\mathrm{eff}}(\Delta\tilde{\nu})$ curves for bandwidth-limited (dashed line) and chirped (dash-dotted line) pulses are included

in Fig. 5. The picosecond pump pulses may be selected in the rising part of the pulse train in order to avoid severe spectral broadening by self-phase modulation [33].

The walk-off angle α_1 (11) limits the interaction length of the ooe→e phase-matched third harmonic generation. For the situation of phasematching ($\Delta k=0$) the reduction of energy conversion due to the finite beam diameter Δd (FWHM) is approximately given by ($r_0=\Delta d/\{2[\ln(2)]^{1/2}\}$):

$$\frac{\eta(\Delta d)}{\eta(\infty)}=\frac{\int_0^l Z\int_{-\infty}^{\infty}\exp\{-[2Y^2+(Y+\alpha_1 Z)^2]/r_0^2\}dY\,dZ}{\int_0^l Z\int_{-\infty}^{\infty}\exp[-3Y^2/r_0^2]dY\,dZ}$$

$$=\frac{3\Delta d^2}{8\ln(2)\alpha_1^2 l^2}\left[1-\exp\left(-\frac{8\ln(2)\alpha_1^2 l^2}{3\Delta d^2}\right)\right]. \quad (35)$$

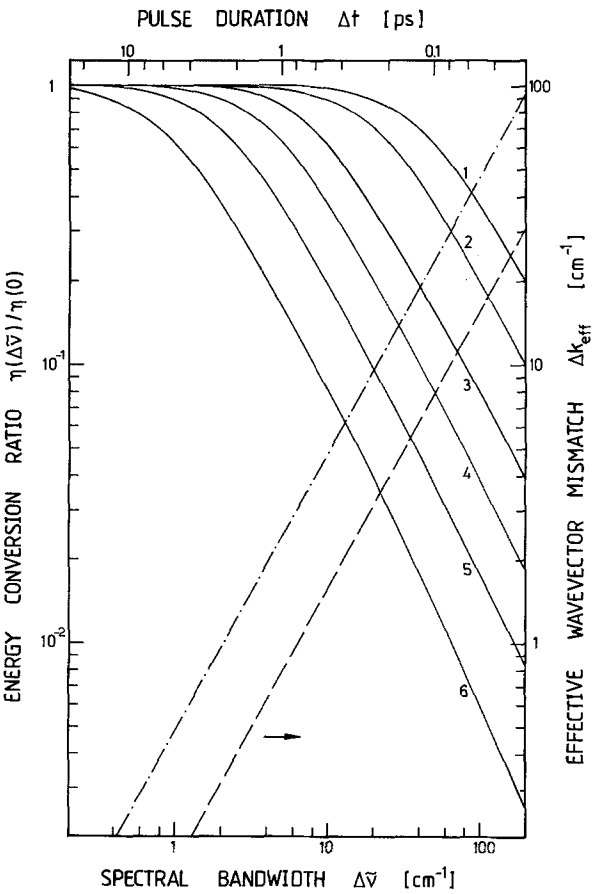

Fig. 5. Reduction of third-harmonic energy conversion efficiency by spectral bandwidth of pump pulse $\Delta\bar{\nu}$ for type-II phase-matching. The solid curves versus the lower abscissa belong to chirped pulses, while the solid curves versus the upper abscissa belong to the bandwidth limited pulses. Curves *1* $l=0.1$ cm; *2* $l=0.2$ cm; *3* $l=0.5$ cm; *4* $l=1$ cm; *5* $l=2$ cm; *6* $l=5$ cm. The effective wave-vector mismatch due to spectral bandwidth is included. The dashed curve belongs to bandwidth-limited pulses and the dash-dotted curve is responsible for chirped pulses. $\lambda_1=1.054\,\mu$m

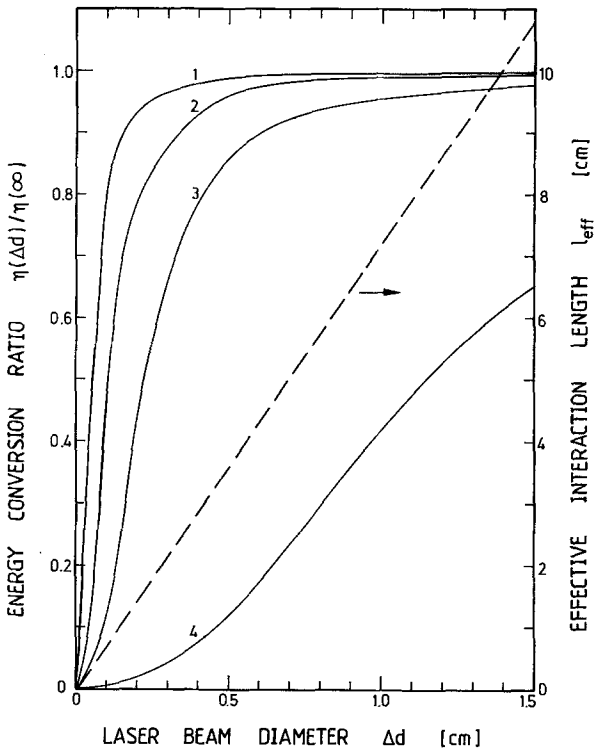

Fig. 6. Dependence of third-harmonic conversion efficiency on pump laser beam diameter Δd (FWHM) for type-II phase-matching. Curves *1* $l=0.5$ cm; *2* $l=1$ cm; *3* $l=2$ cm; *4* $l=5$ cm. Effective interaction length versus beam diameter is included [dashed curve, for definition see text and (36)]. $\lambda_1=1.054\,\mu$m

The walk-off angle for ooe→e interaction at $\lambda_1=1.054\,\mu$m is $\alpha_1=5.83°$. $\eta(\Delta d)/\eta(\infty)$ versus Δd is plotted in Fig. 6 for various sample lengths. In case of $\Delta d=5$ mm and $l=2$ cm the reduction of energy conversion efficiency is $\eta(\Delta d)/\eta(\infty)=0.86$. The pump laser may be focused with a cylindrical lens to a line focus along the *Y*-axis in order to increase the pump pulse intensity without reducing the relevant beam diameter.

An effective interaction length, l_{eff}, may be defined by equating the conversion efficiency of a crystal without walk-off angle of length l_{eff} with the conversion efficiency of a infinitely long crystal having a walk-off angle α_1. The effective length is found to be (35)

$$l_{\text{eff}}=\left[\frac{3}{2\ln(2)}\right]^{1/2}\frac{\Delta d}{2\alpha_1} \quad (36)$$

$l_{\text{eff}}(\Delta d)$ is included in Fig. 6 (dashed line). For $\Delta d=5$ mm the effective interaction length is $l_{\text{eff}}=3.6$ cm in case of ooe→e interaction at $\lambda_1=1.054\,\mu$m.

In case of wavevector mismatch, $\Delta k\neq 0$, the walk-off angle loses its importance if the coherence length [19] $l_{\text{coh}}=\pi/|\Delta k|$ becomes less than l_{eff}.

The refractive indices of calcite are temperature dependent. A temperature change of ΔT causes a wave-

vector mismatch $\frac{\partial \Delta k}{\partial T}\Delta T$ and a reduction of third-harmonic energy conversion of

$$\frac{\eta(\Delta T)}{\eta(0)}=\frac{\sin^2\left(\frac{\partial \Delta k}{\partial T}\Delta T l/2\right)}{\left(\frac{\partial \Delta k}{\partial T}\Delta T l/2\right)^2}. \tag{37}$$

The temperature derivative is approximately $\partial \Delta k/\partial T \simeq -6\times10^{-4}\,\mathrm{cm}^{-1}/\mathrm{K}$ (ooe→e, $\lambda_1=1.054\,\mu\mathrm{m}$, $T=20\,^\circ\mathrm{C}$, (9) with $n(T+\Delta T)=n(T)+\frac{\partial n}{\partial T}\Delta T$, $\frac{\partial n}{\partial T}$ from [23]). This value is negligibly small.

The energy conversion as a function of crystal orientation (ooe→e interaction) is depicted in Fig. 7. The curves are normalized to $\eta(\theta_{II}, \Delta\theta=0, \Delta\tilde{\nu}_1=0)$. A crystal length of $l=2$ cm is used. The influence of the walk-off angle is not included. Curve 1 is calculated for $\Delta\theta=0$ (parallel light beam) and $\Delta\tilde{\nu}=0$ (monochromatic light) by use of (21b)

$$[\eta(\theta)/\eta(\theta_{II})=\sin^2(\Delta k l/2)/(\Delta k l/2)^2].$$

The curves 2–7 belong to increasing beam divergence $\Delta\theta$ and $\Delta\tilde{\nu}=0$. The curves 8–12 are calculated for $\Delta\theta=0$ and rising spectral bandwidth $\Delta\tilde{\nu}$ of bandwidth-limited pulses ($\partial\Delta k'/\partial\tilde{\nu}=0.46$). The curves are calculated by generalizing the relations (31) and (33) to

$$\frac{\eta(\theta,\Delta\theta,\Delta\tilde{\nu})}{\eta(\theta_{II},0,0)}=\frac{\int_{-\infty}^{\infty}d\theta'\exp\left(-\frac{\theta'^2}{\theta_0^2}\right)\int_{-\infty}^{\infty}d\tilde{\nu}'\exp\left(-\frac{\tilde{\nu}'^2}{\tilde{\nu}_0^2}\right)\frac{\sin^2\left[\left(\Delta k_0+\frac{\partial\Delta k}{\partial\theta'}\theta'+\frac{\partial\Delta k'}{\partial\tilde{\nu}}\tilde{\nu}'\right)l/2\right]}{\left[\left(\Delta k_0+\frac{\partial\Delta k}{\partial\theta'}\theta'+\frac{\partial\Delta k'}{\partial\tilde{\nu}'}\tilde{\nu}'\right)l/2\right]^2}}{\int_{-\infty}^{\infty}d\theta'\exp\left(-\frac{\theta'^2}{\theta_0^2}\right)\int_{-\infty}^{\infty}d\tilde{\nu}'\exp\left(-\frac{\tilde{\nu}'^2}{\tilde{\nu}_0^2}\right)}. \tag{38}$$

The oscillations for $\Delta\theta=0$ and $\Delta\tilde{\nu}=0$ are lost readily for increasing $\Delta\theta$ and $\Delta\tilde{\nu}$-values and the half widths of the angular tuning curves broaden while the conversion peak at $\theta=\theta_{II}$ reduces.

In Fig. 8 some realistic angular energy conversion tuning curves for the combined action of $\Delta\theta$ and $\Delta\tilde{\nu}$ are depicted and experimental points are included (see below). The curves belong to chirped pulses ($\partial\Delta k'/\partial\tilde{\nu}=1.38\times10^{-4}\,\mathrm{cm}^{-1}/\mathrm{rad}$) except curve 1 (bandwidth limited, $\Delta\tilde{\nu}=3\,\mathrm{cm}^{-1}$).

The interaction length is limited by the wavevector mismatches due to divergence and spectral width and due to the walk-off angle. For nondivergent ($\Delta\theta\to0$), bandwidth limited pulses of large beam diameter the group-velocity dispersion may be the limiting factor for the interaction length. The group refractive index is given by [35]

$$n_g=\frac{n}{1-\frac{\tilde{\nu}}{n}\frac{\partial n}{\partial\tilde{\nu}}}. \tag{39}$$

The time delay per unit length between ordinary and extraordinary ray of the pump pulse is $(\delta t/\delta l)_{o1e1}=(n_{go1}-n_{ge1}(\theta))/c_0=1.56$ ps/cm at $\lambda_1=1.054\,\mu$m. The overlap length, l_{over}, for a pump pulse of duration Δt_1 (FWHM) is

$$l_{over}\simeq\frac{\Delta t}{(\delta t/\delta l)_{o1e1}} \tag{40}$$

l_{over} versus Δt is plotted in Fig. 9a.

The group velocity dispersion broadens the duration of the third-harmonic light. Without group velocity dispersion the duration of the third harmonic light is $\Delta t_3=\Delta t/3^{1/2}$ [(20); $I_3\propto I_1^3\propto\exp(-3t^2/t_0^2)$] as long as no pump pulse depletion occurs. The time delay per unit length between the third harmonic light and the ordinary ray of the pump pulse is $(\delta t/\delta l)_{e3o1}\simeq2.6$ ps/cm. This time spreading between the third-harmonic light and the pump pulse broadens the third-harmonic pulse duration to

$$\Delta t_3\simeq[\tfrac{1}{3}\Delta t^2+(\delta t/\delta l)_{e3o1}^2 l'^2]^{1/2} \tag{41}$$

l' is the shorter of the lengths l and l_{over}. The approximate third-harmonic pulse durations versus crystal length are shown in Fig. 9b for two different pump pulse durations.

2. Experimental

The experimental setup is shown in Fig. 10. A passively modelocked Nd:phosphate glass laser is used which generates picosecond pulses of about 5 ps duration at 1.054 μm [33]. A single pulse is selected from the pulse train with an electro-optical switch. The separated pulse is amplified in a double-passage through a Nd:phosphate glass amplifier. In some experiments a second Nd:phosphate glass amplifier was applied. The pump pulse divergence and the beam diameter are measured with the diode array systems DA1 and DA2.

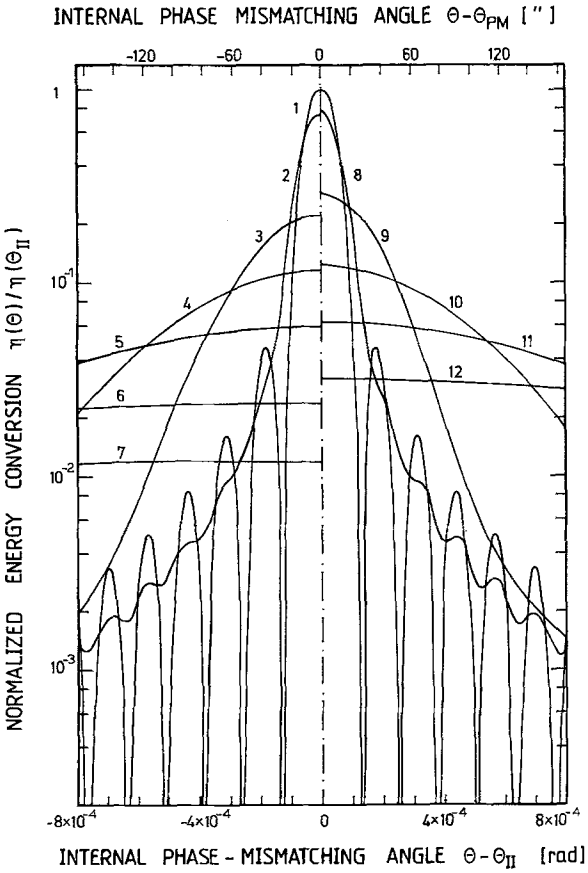

Fig. 7. Normalized energy conversion efficiency versus internal phase-mismatching angle for type-II interaction. Curves *1–7*: $\Delta\tilde{\nu}=0$ with (*1*) $\Delta\theta=0$, (*2*) $\Delta\theta=10^{-4}$ rad, (*3*) $\Delta\theta=5\times10^{-4}$ rad, (*4*) $\Delta\theta=10^{-3}$ rad, (*5*) $\Delta\theta=2\times10^{-3}$ rad, (*6*) $\Delta\theta=5\times10^{-3}$, and (*7*) $\Delta\theta=10^{-2}$ rad. Curves *8–12*: $\Delta\theta=0$ with (*8*) $\Delta\tilde{\nu}_1=5\,\mathrm{cm}^{-1}$, (*9*) $\Delta\tilde{\nu}_1=20\,\mathrm{cm}^{-1}$, (*10*) $\Delta\tilde{\nu}_1=50\,\mathrm{cm}^{-1}$, (*11*) $\Delta\tilde{\nu}_1=100\,\mathrm{cm}^{-1}$, and (*12*) $\Delta\tilde{\nu}=200\,\mathrm{cm}^{-1}$. Curves are calculated for bandwidth-limited pulses. $\lambda_1=1.054\,\mu\mathrm{m}$

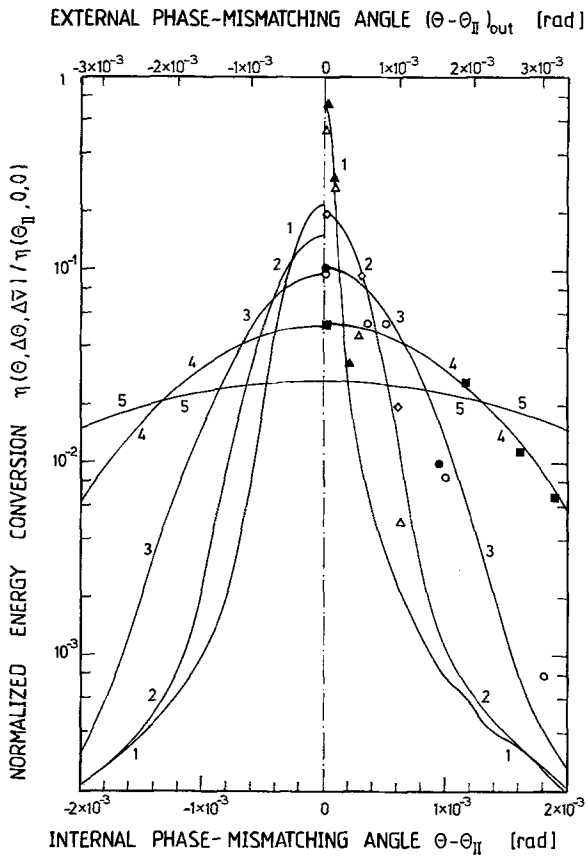

Fig. 8. Normalized energy conversion efficiency versus internal (lower abscissa) and external phase-mismatching angle (upper abscissa) for type-II interaction in calcite. Left half: $\Delta\theta=5\times10^{-4}$ rad; right half: $\Delta\theta=1\times10^{-4}$ rad. Curves *1* are band-with limited with $\Delta\tilde{\nu}_1=3\,\mathrm{cm}^{-1}$. The other curves are chirped with (*2*) $\Delta\tilde{\nu}_1=10\,\mathrm{cm}^{-1}$, (*3*) $\Delta\tilde{\nu}_1=20\,\mathrm{cm}^{-1}$, (*4*) $\Delta\tilde{\nu}_1=40\,\mathrm{cm}^{-1}$, and (*5*) $\Delta\tilde{\nu}_1=80\,\mathrm{cm}^{-1}$. The filled points belong to azimuthal angle $\phi=90°$. The open points belong to $\phi=270°$. (△): $\Delta\tilde{\nu}\cong5\,\mathrm{cm}^{-1}$; (◇): $\Delta\tilde{\nu}\cong10\,\mathrm{cm}^{-1}$; (○): $\Delta\tilde{\nu}\cong20\,\mathrm{cm}^{-1}$; (□): $\Delta\tilde{\nu}\cong40\,\mathrm{cm}^{-1}$

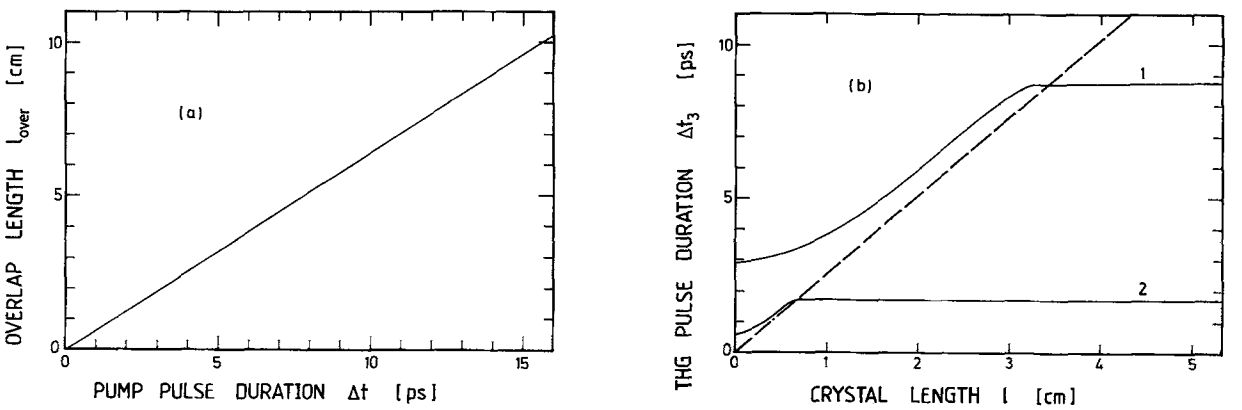

Fig. 9. (a) Overlap length between ordinary and extraordinary ray of pump pulse versus pump pulse duration in calcite $\lambda_1=1.054\,\mu\mathrm{m}$. $(\delta t/\delta l)_{o1e1}=1.56\,\mathrm{ps/cm}$. (b) Broadening of pulse duration of third harmonic light in calcite crystal due to group velocity dispersion. $\lambda_1=1.054\,\mu\mathrm{m}$, $(\delta t/\delta l)_{e3o1}=2.6\,\mathrm{ps/cm}$. Solid curves belong to (*1*) $\Delta t=5\,\mathrm{ps}$ and (*2*) $\Delta t=1\,\mathrm{ps}$. Dashed curve gives time delay between extraordinary ray at λ_3 and ordinary ray at λ_1

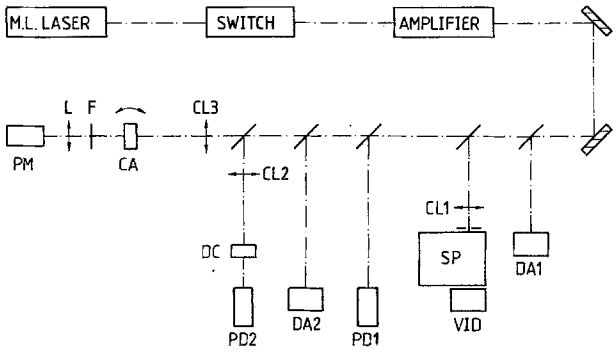

Fig. 10. Experimental arrangement. DA1 and DA2, linear diode arrays. CL1–CL3, cylindrical lenses. SP, 30 cm grating spectrometer. VID, vidicon of optical spectrum analyser. PD1 and PD2, vacuum photodetectors. DC, saturable absorber cell for intensity detection. CA, calcite crystal. F, filters. L, lens. PM, photomultiplier

The spectral distribution of the pump pulses is registered with a spectrometer SP and a vidicon system VID (optical spectrum analyser). The input pulse peak intensity is determined by nonlinear transmission measurements through a saturable absorber DC [36] (Kodak dye No. 9860 in 1,2-dichloroethane) with photodetectors PD2 and PD1.

The third-harmonic light is generated in the angle tuned calcite crystal CA. Type-II phase-matching is applied ($\theta_{II}=35.96°$). The azimuthal angles $\phi=90°$ and $\phi=270°$ are used. The angle β between pump pulse field strength $\mathbf{E}_1$ and X-axis is $\beta=\text{arccotan}(2)=26.57°$ (optimum condition, see above). The crystal length is $l=2$ cm. In some experiments the input pump pulse intensity is increased by forming a line focus in the YZ-plane with a cylindrical lens CL3 (increase of intensity withouth an increase of relevant beam divergence). The generated third harmonic light is detected with the photomultiplier PM. The energy conversion efficiency η is determined by calibrating the photomultiplier PM to the photodetector PD1.

3. Results

The experimental points in Fig. 8 show the angular dependence of the third-harmonic signal. The lower abscissa gives the phase-mismatching angle inside the crystal. The upper abscissa presents the external phase-mismatching angle outside the crystal $[(\theta-\theta_{II})_{\text{out}} \simeq n_{o1}(\theta-\theta_{II})]$. The filled points belong to $\phi=90°$ and the open points belong to $\phi=270°$. The circles are adjusted to the calculated curve of $\Delta\theta=10^{-4}$ rad and $\Delta\tilde{\nu}=20\,\text{cm}^{-1}$. The measured points fit well to the calculated curves. The measured pump beam divergence is in the region between 10^{-4} rad and 5×10^{-4} rad. The applied beam diameter was approximately 5 mm. The spectral width of the pump pulses

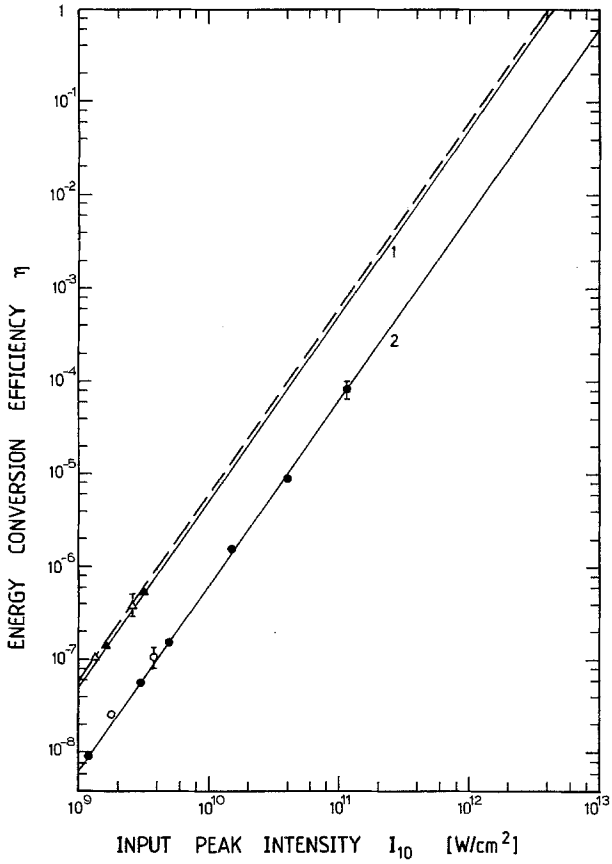

Fig. 11. Third-harmonic energy conversion efficiency versus input pump pulse peak intensity. Type-II phase-matching is applied. Crystal length $l=2$ cm. Pump laser wavelength $\lambda_1=1.054\,\mu$m. Filled points belong to azimuthal angle $\phi=90°$. Open points belong to $\phi=270°$. Curve *1* and triangles: $\Delta\theta=1\times10^{-4}$, $\Delta\tilde{\nu}=5\,\text{cm}^{-1}$ and $\Delta d=5$ mm. Curve *2* and circles: $\Delta\theta=1\times10^{-4}$ rad, $\Delta\tilde{\nu}=20\,\text{cm}^{-1}$ and $\Delta d=5$ mm. Dashed curve: $\Delta\theta=0$, $\Delta\tilde{\nu}=0$, and $\Delta d\to\infty$. The curves are calculated (21b) with $\chi^{(3)}_{\text{eff},II}(\phi=90°)=\chi^{(3)}_{\text{eff},II}(\phi=270°)=3\times10^{-24}\,\text{m}^2\,\text{V}^{-2}$

was varied by changing the position of the selected single pulse within the pulse train.

In Fig. 11 the energy conversion η at the phase-matching angle θ_{II} is plotted versus input pulse peak intensity I_{10}. The open points belong to the azimuthal angle $\phi=270°$. The filled points belong to $\phi=90°$. Within the experimental accuracy the energy conversion efficiency for $\phi=90°$ and $\phi=270°$ is the same. The solid curves are fitted to the experimental points. The dashed curve belongs to $\Delta\tilde{\nu}=0$ and $\Delta\theta=0$. The fitting parameter is the effective nonlinear susceptibility. Its value is $\chi^{(3)}_{\text{eff},II}(\phi=90°)=\chi^{(3)}_{\text{eff},II}(\phi=270°)=(3.0\pm0.6)\times10^{-24}$ m^2 V^{-2} $=(2.15\pm0.5)\times10^{-16}$ esu (1 esu $=(9\times10^8/4\pi)\text{m}^2\,\text{V}^{-2}$ [26]).

For our experimental systems the highest obtainable pulse intensity was about $10^{11}\,\text{W/cm}^2$. It was achieved by using a cylindrical length of 30 cm focal length and by selecting pulses from the pulse train

maximum ($\Delta\tilde{\nu} \simeq 20\,\mathrm{cm}^{-1}$). The relevant beam diameter in the ZY-plane remained $\Delta d \simeq 5\,\mathrm{mm}$. The highest conversion efficiency was about 1×10^{-4}.

4. Discussion

The effective third-order nonlinear optical susceptibility $\chi^{(3)}_{\mathrm{eff},II}$ contains the three independent susceptibility components χ_{11}, $\chi_{10} = \chi_{39}$, and χ_{35}. χ_{11} has been determined previously by non-phase-matched third-harmonic generation [19] ($\mathbf{E}_1 \perp c$-axis, $\mathbf{k}_1 \perp c$-axis). A value of $\chi_{11} = 5.2 \times 10^{-23}\,\mathrm{m}^2\,\mathrm{V}^{-2}$ has been obtained. Using χ_{11} of [19] and $\chi^{(3)}_{\mathrm{eff},II}(90°) \simeq \chi^{(3)}_{\mathrm{eff},II}(270°)$ of this work the susceptibility components χ_{10} and χ_{35} are found to be $|\chi_{10}| = (0 \pm 5 \times 10^{-25})\,\mathrm{m}^2\,\mathrm{V}^{-2}$ and $\chi_{35} \simeq -6.5 \times 10^{-24}\,\mathrm{m}^2\,\mathrm{V}^{-2}$. The values of the susceptibility components are not very accurate because of the uncertainties of the effective susceptibilities.

In our experiments we were limited to input pulse peak intensities $I_{10} \leqq 10^{11}\,\mathrm{W/cm}^2$. The focusing with the cylindrical lens did not lead to higher intensities. The damage threshold peak intensity I_{th} was determined by focusing with a spherical lens into the crystal. The damage threshold was found to be $I_{10,\mathrm{th}} > 10^{13}\,\mathrm{W/cm}^2$ for single picosecond pump pulses of about 5 ps duration (no surface and no bulk damage observed for $I_{10} \leqq 10^{13}\,\mathrm{W/cm}^2$). Increasing the pump pulse peak intensity to $I_{10} = 2 \times 10^{12}\,\mathrm{W/cm}^2$ would lead to an energy conversion efficiency of $\eta \simeq 0.20$ for band-width limited pulses ($\Delta\theta = 1 \times 10^{-4}$, $\Delta\tilde{\nu} \simeq 3\,\mathrm{cm}^{-1}$, $\Delta d \simeq 5\,\mathrm{mm}$, $l = 2\,\mathrm{cm}$). For high power picosecond lasers, as used for laser fusion experiments [37], calcite should be an useful crystal for efficient direct third-harmonic generation.

5. Conclusions

The direct third-harmonic generation in calcite suffers from the very small effective third-order nonlinear susceptibility and the large walk-off angle. The damage threshold of the crystal is very high for picosecond pump pulses ($I_{10,\mathrm{th}} > 10^{13}\,\mathrm{W/cm}^2$). The application of non-divergent, bandwidth-limited, large-diameter picosecond pump pulses of intensities in the $\mathrm{TW/cm}^2$ region offers the possibility of efficient third-harmonic generation with energy conversions in the ten percent region.

Acknowledgements. The authors thank Th. Ascherl for technical assistance and the Rechenzentrum of the University of Regensburg for provision of computer time. P.Q. is very grateful to the Alexander von Humboldt-Stiftung for a fellowship.

References

1. R. Piston: Laser Focus **14**/7, 66 (1978)
2. R. Gonzales, M.A. Henesian, D. Milam, C.L. Weinzapfel: Laser Program Annual Report 84, Lawrence Livermore National Laboratory, Livermore, Calif., UCRL-50021-84 (1984) pp. 6–50
3. D. Eimerl: IEEE J. QE-**23**, 575 (1987)
4. J.F. Reintges: *Nonlinear Parametric Processes in Liquids and Gases* (Academic, Orlando 1984)
5. J.F. Reintges: In *Laser Handbook*, Vol. 5, ed. by M. Bass, M.L. Stitch (North-Holland, Amsterdam 1985) Chap. 1
6. C.R. Vidal: In *Tunable Lasers*, ed. by L.F. Mollenauer, J.C. White, Topics in Appl. Phys. Vol. 59 (Springer, Berlin, Heidelberg 1987) pp. 57
7. P.P. Bey, J.F. Galbraith, H. Rabin: IEEE J. QE-7, 86 (1971)
8. J.C. Diels, F.P. Schäfer: Appl. Phys. **5**, 197 (1974)
9. W. Leupacher, A. Penzkofer, B. Runde, K.H. Drexhage: Appl. Phys. B **44**, 133 (1987)
10. A. Penzkofer, W. Leupacher: Opt. Quant. Electron. **20** (1988) (to be published)
11. P.D. Maker, R.W. Terhune, C.M. Savage: *Proceedings of the Third Conf. on Quantum Electronics, Paris (1983)*, ed. by P. Grivet, N. Bloembergen (Columbia University Press, New York 1964) p. 1559
12. C.C. Wang, E.L. Baardsen: Appl. Phys. Lett. **15**, 396 (1969)
13. S.A. Akhmanov, L.B. Meisner, S.T. Parinov, S.M. Saltiel, V.G. Tunkin: Sov. Phys. JETP **46**, 898 (1977)
14. R.W. Terhune, P.D. Maker, C.M. Savage: Appl. Phys. Lett. **2**, 54 (1963)
15. P.D. Maker, R.W. Terhune: Phys. Rev. **137** A, 801 (1965)
16. P. Sukhorukov, I.V. Tomov: Sov. Phys. JETP **31**, 872 (1970)
17. Y.R. Shen: *The Principles of Nonlinear Optics* (Wiley, New York 1984)
18. M. Schubert, B. Wilhelmi: *Nonlinear Optics and Quantum Electronics* (Wiley, New York 1986)
19. M. Thalhammer, A. Penzkofer: Appl. Phys. B **32**, 137 (1983)
20. J.A. Armstrong, N. Bloembergen, J. Ducuing, P.S. Pershan: Phys. Rev. **127**, 1918 (1962)
21. F. Zernike, J.E. Midwinter: *Applied Nonlinear Optics* (Wiley, New York 1973)
22. P.N. Butcher: *Nonlinear Optical Phenomena*, Bulletin 200, Engineering Experiment Station, Ohio State University (Columbus, Ohio 1965)
23. *American Institute of Physics Handbook*, 3rd edn., ed. by D.E. Gray (McGraw-Hill, New York 1972) pp. 6–20
24. J.E. Midwinter, J. Warner: Br. J. Appl. Phys. **16**, 1667 (1965)
25. D.E. McCarthy: Appl. Opt. **6**, 1896 (1967)
26. R.W. Minck, R.W. Terhune, C.C. Wang: Appl. Opt. **5**, 1595 (1966)
27. D.A. Kleinman: Phys. Rev. **126**, 1977 (1962)
28. J.E. Bjorkholm, A.E. Siegman: Phys. Rev. **154**, 851 (1967)
29. F. Shimizu: Phys. Rev. Lett. **19**, 1097 (1967)
30. T.K. Gustanfson, J.P. Taran, H.A. Haus, J.R. Lifshitz, P.L. Kelly: Phys. Rev. **177**, 306 (1969)
31. S.A. Akhmanov, R.V. Khokhlov, A.P. Sukhorukov: In *Laser Handbook*, Vol. 2, ed. by F.T. Arrecchi, E.O. Schulz-Dubois (North-Holland, Amsterdam 1972) Chap. E3
32. R.C. Eckhardt, C.H. Lee, J.N. Bradford: Opto-Electron. **6**, 67 (1974)
33. A. Penzkofer, F. Graf: Opt. Quant. Electron. **17**, 219 (1985)
34. J. Herrmann, B. Wilhelmi: *Laser für ultrakurze Lichtimpulse* (Physik Verlag, Weinheim 1984) p. 84
35. E. Hecht, A. Zajac: *Optics* (Addison-Wesley, Reading, Mass. 1974)
36. A. Penzkofer, D. von der Linde, A. Laubereau: Opt. Commun. **4**, 377 (1972)
37. J.L. Emmett, W.F. Krupke, J.I. Davis: IEEE J. QE-**20**, 591 (1984)